



Article

On-Board Liquid Hydrogen Cold Energy Utilization System for a Heavy-Duty Fuel Cell Hybrid Truck

Mingye Yang¹, Song Hu^{1,2,*} , Fuyuan Yang^{1,*}, Liangfei Xu¹, Yu Bu³ and Dian Yuan⁴

¹ State Key Laboratory of Automotive Safety and Energy, Tsinghua University, Beijing 100084, China; 18811613072@163.com (M.Y.); xuliangfei@tsinghua.edu.cn (L.X.)

² School of Mechanical Engineering, University of Science and Technology Beijing, Beijing 100083, China

³ Beijing Institute of Aerospace Testing Technology, Beijing 100071, China; coffee850129@163.com

⁴ Beijing SinoHytec Co., Ltd., Haidian Distract, Beijing 100084, China; yuandian@autoht.com

* Correspondence: husong_90@163.com (S.H.); fyyang@tsinghua.edu.cn (F.Y.)

Abstract: In this paper, a kind of on-board liquid hydrogen (LH₂) cold energy utilization system for a heavy-duty fuel cell hybrid truck is proposed. Through this system, the cold energy of LH₂ is used for cooling the inlet air of a compressor and the coolant of the accessories cooling system, sequentially, to reduce the parasitic power, including the air compressor, water pump, and radiator fan power. To estimate the cold energy utilization ratio and parasitic power saving capabilities of this system, a model based on AMESim software was established and simulated under different ambient temperatures and fuel cell stack loads. The simulation results show that cold energy utilization ratio can keep at a high level except under extremely low ambient temperature and light load. Compared to the original LH₂ system without cold energy utilization, the total parasitic power consumption can be saved by up to 15% (namely 1.8 kW).

Keywords: hydrogen; energy recovery; heat exchange; heavy-duty; fuel cell vehicle



Citation: Yang, M.; Hu, S.; Yang, F.; Xu, L.; Bu, Y.; Yuan, D. On-Board Liquid Hydrogen Cold Energy Utilization System for a Heavy-Duty Fuel Cell Hybrid Truck. *World Electr. Veh. J.* **2021**, *12*, 136. <https://doi.org/10.3390/wevj12030136>

Academic Editor: Michael Fowler

Received: 22 July 2021

Accepted: 25 August 2021

Published: 27 August 2021

Publisher's Note: MDPI stays neutral with regard to jurisdictional claims in published maps and institutional affiliations.



Copyright: © 2021 by the authors. Licensee MDPI, Basel, Switzerland. This article is an open access article distributed under the terms and conditions of the Creative Commons Attribution (CC BY) license (<https://creativecommons.org/licenses/by/4.0/>).

1. Introduction

With the development of the fuel cell electric vehicle (FCEV), there has been an increasing demand for a hydrogen source with high energy density. The common hydrogen sources of on-board hydrogen storage and supply systems are high-pressure hydrogen (35 MPa and 70 MPa), low-temperature liquid hydrogen (LH₂), and metal hydride [1,2]. Among them, the first two methods are more commonly used. Furthermore, the density of liquid hydrogen (10 bar, 31 K, 50 kg/m³) is about 2.2 times higher than that of 35 MPa high-pressure gas hydrogen (23 kg/m³) at room temperature, and 1.35 times that of 70 MPa gas hydrogen (37 kg/m³) at room temperature [3]. As for the liquid hydrogen tank, its weight density is at least 9 wt%, while these examples of 35 MPa and 70 MPa hydrogen storage solutions are just 2.5 wt% and 4.5 wt%, respectively. In addition, the storage and transportation costs of liquid hydrogen are also much lower than compressed hydrogen [4]. Therefore, liquid hydrogen is widely considered a competitive hydrogen source, especially for heavy-duty, long-distance vehicles. However, the liquefaction process consumes a large amount of energy, which is the main drawback of LH₂. The actual specific energy consumption of liquefaction is typically about 12–15 kWh per kg LH₂ [5,6], and that of an advanced process could reach about 5–6 kWh per kg LH₂ [7,8]. In order to increase the overall efficiency of LH₂, it is important to recover part of the liquefaction energy.

As for the cold energy utilization, there has been some research in the field of liquid natural gas (LNG), which has been widely used in energy storage and is similar to LH₂ in its physical properties. LNG cold energy is mainly utilized for air separation, desalination processes, cryogenic carbon dioxide capture, and power generation [9]. More specifically, there are several power generation cycles, including the gas turbine cycle, organic Rankine cycle, Brayton cycle, and combined cycle [10]. Liu et al. proposed an innovative combined

cooling, heating, and power system (CCHP) based on the SOFC/GT/CO₂ cycle and the organic Rankine cycle with LNG cold energy utilization to achieve cascade energy utilization and carbon dioxide capture. The results illustrated that the comprehensive energy utilization, the net power generation, and the overall exergy efficiencies of the system could reach about 79.48%, 79.81%, and 62.29%, respectively [11]. However, these systems are mainly designed for large regasification terminals, and the applications are not consistent with the requirements of vehicles.

Due to the lack of large application, little research have focused on the cold energy utilization of LH₂. Trevisani et al. proposed and compared gas turbine and magnetohydrodynamics based energy recovery systems that produce electric energy [12]. Zhang et al. established a novel Brayton cycle with the integration of LH₂ cryogenic exergy utilization, which can reach high energy and exergy efficiency (73% and 45%, respectively) [13]. However, these systems need gas turbines and additional working fluids, which make them difficult to realize for their on-board application. Few researchers have been able to draw on any systematic research into on-board liquid hydrogen cold energy utilization systems adapted vehicles using LH₂ as fuel.

In this paper, a kind of on-board liquid hydrogen cold energy utilization system is proposed. Considering the cooling demand of fuel cell vehicles and the restriction of space and engineering feasibility, the cold energy of LH₂ in the evaporation process is directly used for cooling the inlet air of compressor and the coolant of the accessories cooling system through a vaporizer to reduce the parasitic power, including the air compressor, water pump, and radiator fan power. Then, the cold energy utilization ratio and parasitic power saving capabilities under different ambient temperatures and fuel cell stack loads are compared and analyzed.

2. Configuration Design

In our previous studies [4], a kind of LH₂ system, named as the original LH₂ system, is proposed and produced; moreover, it has been applied in heavy-duty fuel cell hybrid trucks. The scheme and equipment of original LH₂ systems are respectively shown in Figures 1 and 2. As for this system, the vaporizer consists of two parts, namely the heat exchanger 1 (HEX-1) and heat exchanger 2 (HEX-2). LH₂ firstly passes through HEX-1 and be heated directly by the ambient air to reach from about −40 °C to 20 °C. Then, H₂ passes through HEX-2 and be further heated by the coolant in the accessories cooling system. HEX-2 is necessary for the system because H₂ from the outlet of HEX-1 cannot maintain a proper temperature due to the great change of ambient temperature in different seasons. The accessories cooling system takes away the heat of the DC/DC and compressed air, and releases it to low temperature H₂ and the environment. According to a previous joint test of this system and the fuel cell system, the liquid hydrogen system had the ability to keep the pressure relatively stable at different working conditions and could meet the gas supply requirements of the fuel cell stack [4]. However, unfortunately, a large amount of LH₂ cold energy is not utilized but rather dissipated to the environment through HEX-1, which decreases the overall efficiency of the LH₂ supply chain.

In order to recover the energy spent for liquefaction, a kind of on-board liquid hydrogen cold energy utilization system is proposed, as shown in Figure 3. Different from the original LH₂ system, the LH₂ from the tank firstly passes through HEX-1 to cool the inlet air of the air compressor, rather than the ambient air, and thus reduces the power consumption of the compressor. In addition, the load of the intercooler is also reduced, which is beneficial, owing to the size reduction of intercooler. H₂ also needs to pass through HEX-2 to be further heated by the coolant. This process cools the coolant and thus the water pump power and the radiator fan power can be reduced. In other words, HEX-2 serves as a radiator for the accessories cooling system. However, the cold energy transferred to the system may exceed the cooling demand under low ambient temperature. Therefore, an electric heater is used to maintain the coolant temperature, which eventually keeps the temperature of the fuel cell stack inlet of H₂ and air within proper range.

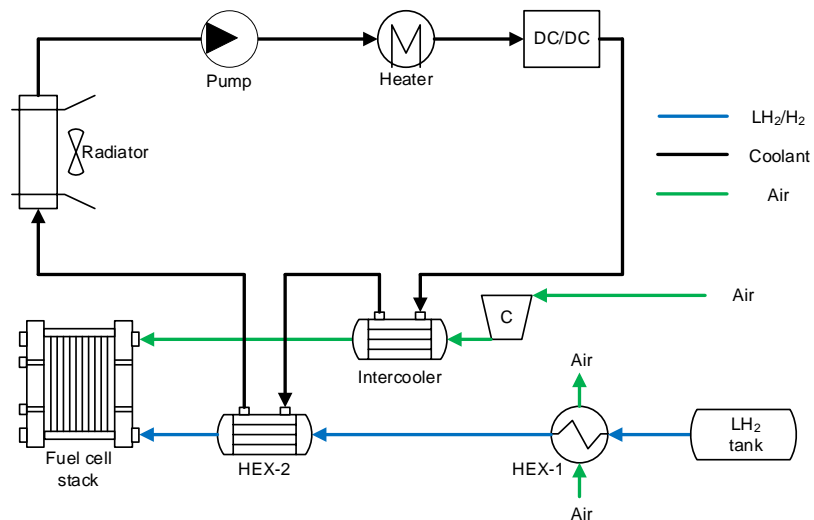


Figure 1. Scheme of original LH₂ system.



Figure 2. Equipment of original LH₂ system.

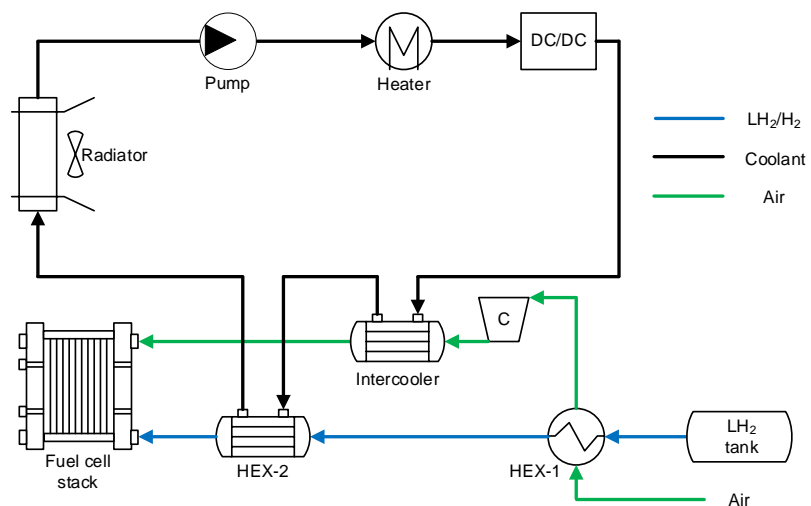


Figure 3. Scheme of LH₂ cold energy utilization system.

3. Methodology

3.1. System Model

To analyze the cold energy and the cooling demand under different working conditions and ambient temperature, a zero-dimensional model was established based on AMESim (Figure 4), which includes four parts: fuel cell stack, H₂ supply subsystem, air supply subsystem, and the accessories cooling subsystem. AMESim is an integrated, scalable system simulation platform and consists of multi-physics libraries, which make it suitable for the modeling of thermal management systems by simulating heat transfer between solids, liquids, and gas, as well as through phase change phenomena [14]. The four subsystems are detailed as follows:

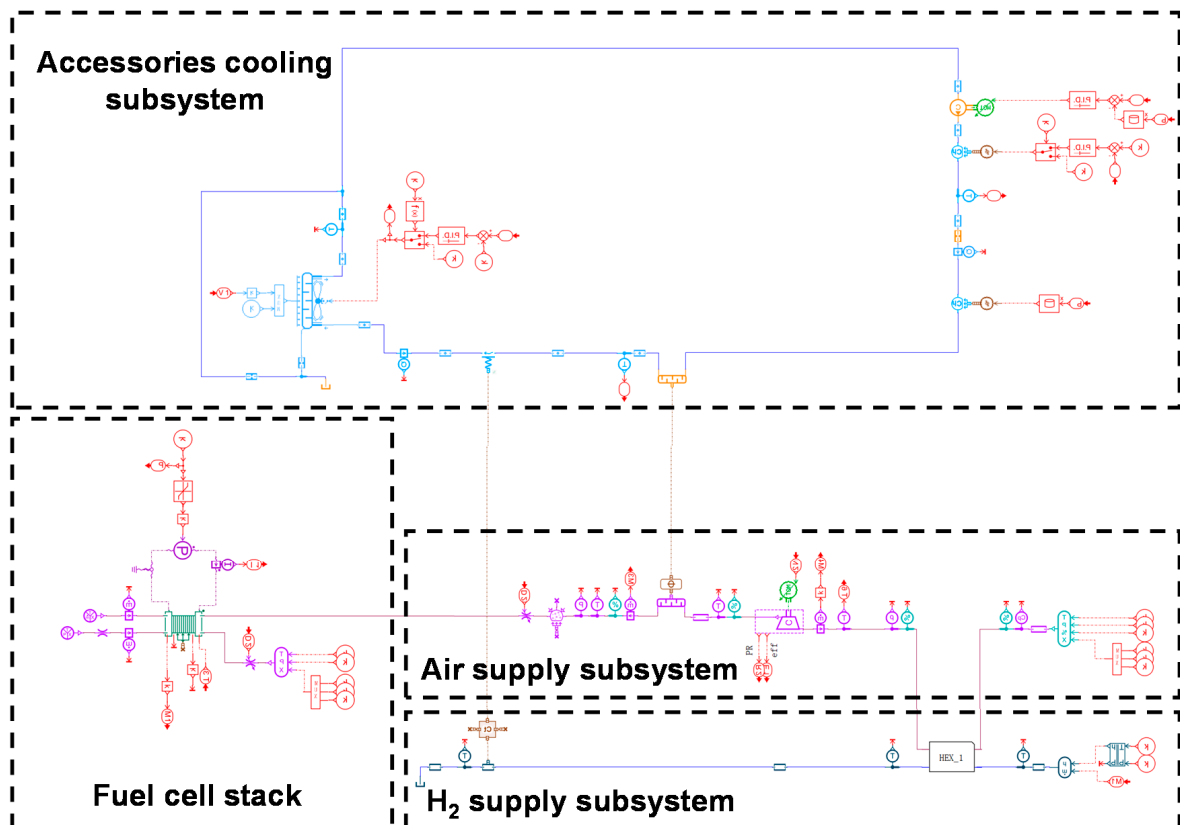


Figure 4. System model in AMESim.

3.1.1. Fuel Cell Stack Model

In this study, a zero-dimensional fuel cell stack model was developed to determine the electric voltage and output power under different current density. The polarization curve was obtained from the following equation:

$$V_{cell} = V_{nernst} - V_{act} - V_{conc} - V_{ohmic} \quad (1)$$

$V_{nernst} = 1.23$ V is Nernst theoretical voltage, V_{act} is activation polarization, V_{conc} is concentration polarization, and V_{ohmic} is ohmic polarization.

Equation (1) is calibrated using experimental data (as shown in Figure 5) and embedded in the AMESim fuel cell module. Therefore, the current and voltage under different fuel cell stack loads can be calculated, which is crucial to determine the maximum LH₂ cold energy.

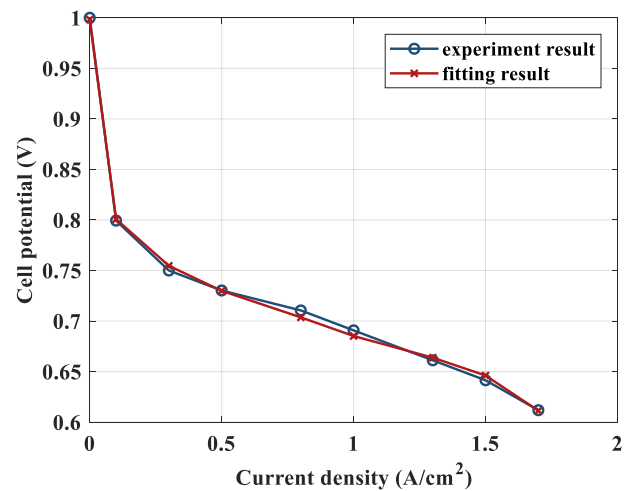


Figure 5. Fuel cell polarization curve calibration.

3.1.2. H₂ Supply Subsystem

H₂ flow rate was determined by the fuel cell stack load and was calculated as follows:

$$\dot{m}_{LH_2} = \frac{N_{cell} I M_{H_2} S_{H_2}}{2F} \quad (2)$$

where N_{cell} is the number of cells in the stack, I is the current of the fuel cell stack, M_{H_2} is relative molecular mass of H₂, $S_{H_2} = 1.05$ is H₂ stoichiometric ratio, and $F = 96,485$ C/mol is Faraday's constant.

The low temperature H₂ sequentially passes through HEX-1 and HEX-2 and exchanges heat with the inlet air of the stack and the coolant of the accessories cooling system.

As for HEX-1 and HEX-2, they were simulated by the convective heat exchange modules in AMESim, and the performance of heat exchangers under different flow rates at room temperature was calibrated by experiments.

3.1.3. Air Supply Subsystem

Air flow rate was also determined by the stack load and was calculated as follows:

$$\dot{m}_{air} = \frac{N_{cell} I M_{O_2} S_{air}}{4F\omega} \quad (3)$$

where M_{O_2} is relative molecular mass of O₂, S_{air} is air stoichiometric ratio, and $\omega = 21\%$ is the mass fraction of O₂ in air. S_{air} varies with fuel cell load (as shown in Figure 6). Under light load (<50%), the stoichiometric ratio should be higher to ensure the basic flow rate and pressure. With the increase of load, the working condition of the fuel cell stack becomes stable, which means that lower stoichiometric ratio could satisfy the requirements of stack. Consequently, S_{air} decreases gradually and remains almost constant after reaching a proper value (about 1.6).

The ambient air was firstly cooled by low temperature H₂ and then compressed by air compressor. The outlet pressure and isentropic efficiency of the air compressor were determined by the map of the compressor, which was tested at different, corrected rotary speeds and corrected air flow rates (as shown in Figure 7).

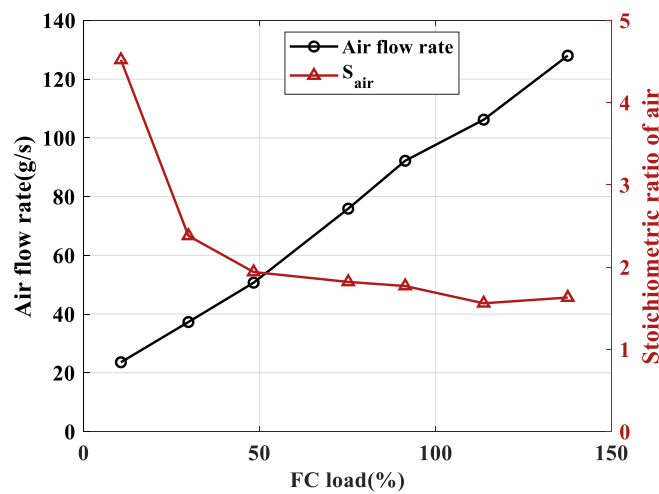


Figure 6. Air flow rate and air stoichiometric ratio under different fuel cell loads.

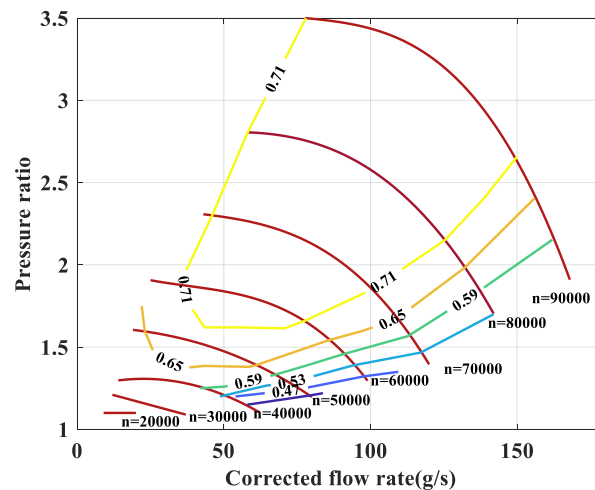


Figure 7. Air compressor performance curves.

3.1.4. Accessories Cooling Subsystem

The accessories cooling subsystem is mainly used to take heat away from DC/DC, intercooler, and other heat generating accessories. The main components include the water pump, PTC heater, DC/DC, intercooler, HEX-2, and radiator. The water pump and radiator fan performance curves were curve-fitted with experiments. Figure 8 shows the heat exchange power of radiator at different coolant flow rates and air flow speeds (the temperature difference of the coolant and air is 25 °C). In addition, the pump flow rate and fan speed are controlled by temperature feedback to ensure that the coolant temperature kept in a proper range.

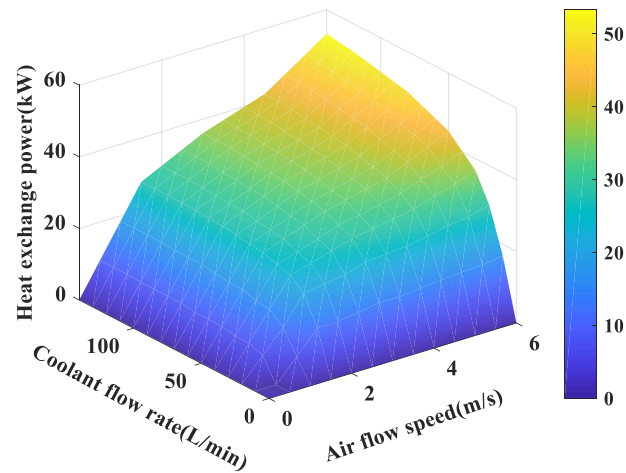


Figure 8. Heat exchange power of radiator at different coolant flow rates and air flow rates.

3.2. Cold Energy Utilization Ratio Analysis

To evaluate the utilization of cold energy under different ambient temperatures and fuel cell stack loads, an index called cold energy utilization ratio was proposed and defined as follows:

$$\eta = \frac{E_{used}}{E_{LH_2}} \quad (4)$$

where E_{used} is the cold energy which is actually used through this system, and E_{LH_2} is the maximum cold energy of LH_2 , which equals the LH_2 enthalpy change from the LH_2 tank (20K) to the inlet of the fuel cell stack (323K). E_{used} contains two parts:

$$E_{used} = E_{comp} + E_{coolant} \quad (5)$$

where E_{comp} is the LH_2 cold energy used for cooling the compressor inlet air and $E_{coolant}$ is the LH_2 cold energy used for cooling the coolant. To be more specific, E_{comp} is calculated as follows:

$$E_{comp} = \min(m_{LH_2}\Delta h_1, E_{demand}), E_{comp} \geq 0 \quad (6)$$

where m_{LH_2} is the mass of liquid hydrogen flow, Δh_1 is the enthalpy change of H_2 in HEX-1, and E_{demand} is the actual cooling demand of the air, which means that, if $m_{LH_2}\Delta h_1$ exceeds the actual cooling demand, the excessive part of cold energy would not be included in E_{comp} . In fact, the excessive part would mean that the outlet air temperature of the compressor is lower than the lowest limiting value. Therefore, the air was heated rather than cooled in the intercooler. Through this process, the excessive cold energy in the HEX-1 is finally exchanged with coolant. Consequently, $E_{coolant}$ was calculated as follows:

$$E_{coolant} = m_{LH_2}\Delta h_2 + E_{extra} - E_{heater}, E_{coolant} \geq 0 \quad (7)$$

$$E_{extra} = m_{LH_2}\Delta h_1 - E_{comp} \quad (8)$$

where Δh_2 is the enthalpy change of H_2 in HEX-2, E_{extra} is the excessive part of the cold energy exchanged in the HEX-1, which exceeds the cooling demand of air, and E_{heater} is the heater power.

3.3. Parasitic Power Analysis

In order to show the effect of LH_2 cold energy more intuitively, the parasitic power of the original system and the cold energy utilization system are calculated and compared. The total parasitic power P_{total} includes four parts:

$$P_{total} = P_{comp} + P_{heater} + P_{fan} + P_{pump} \quad (9)$$

where P_{comp} is air compressor power, P_{heater} is heater power, P_{fan} is radiator fan power, and P_{pump} is water pump power.

4. Results and Discussion

The simulation results achieved under a steady state, including the cold energy utilization ratio and parasitic power savings, were analyzed to evaluate the performance of the LH_2 cold energy utilization system. Some important parameters and boundary conditions are shown in Table 1. In the HEX-1 inlet, the H_2 temperature is assumed to be -220 °C, to simulate the pipe heat loss between the LH_2 tank and vaporizer.

Table 1. Parameters and boundary conditions of cold energy utilization system model.

Parameter	Value
Fuel cell stack nominal power (kW)	100
DC/DC efficiency (%)	95
Fuel cell stack load range (%)	25~100
Ambient temperature range (°C)	-30~40
Ambient humidity (%)	40
Maximum radiator fan power (kW)	0.5
DC/DC inlet coolant temperature control point (°C)	50
HEX-1 inlet H_2 temperature (°C)	-220
Coolant flow rate range (L/min)	50~90

4.1. Cold Energy Utilization Ratio Results

Figure 9 demonstrates the LH_2 cold energy utilization ratio under different ambient temperatures (including -30 °C, -10 °C, 20 °C, and 40 °C) and fuel cell stack loads (25~100%). At a low temperature (<-10 °C, as shown in Figure 9a,b), the cold energy is mainly used for cooling the coolant (accounting for at least 62% of the total utilized cold energy). In addition, the total cold energy utilization ratio is lower than 50% at light load ($<50\%$). The reason for this is that the cooling demand of the system, especially the air pre-cooling demand, is near zero or even negative, due to the low inlet air temperature. Therefore, a part of the cold energy exchanged in HEX-1 and HEX-2 is not actually utilized. While at room temperature and higher (as shown in Figure 9c,d), the cold energy utilization ratio can maintain a high level (about 82%) under different loads, due to the increase of the total cooling demand. Moreover, and different from the results at low temperature, the air pre-cooling part accounts for about 85% of the total utilized cold energy, which indicates that a large part of cold energy is exchanged in HEX-1 and is entirely used for air pre-cooling.

Figure 10a demonstrates the change of η with an ambient temperature and fuel cell stack load. The results show that cold energy utilization ratio increases with temperature and load. Figure 10b shows the contour map of η . It can be seen that the high utilization ratio zone occupies the main part on the whole working range. Specifically, η could reach 80% when the ambient temperature was above -10 °C and could keep above 80% in the whole load range when the temperature was above 20 °C, which indicates that the majority of LH_2 cold energy could be utilized through this system.

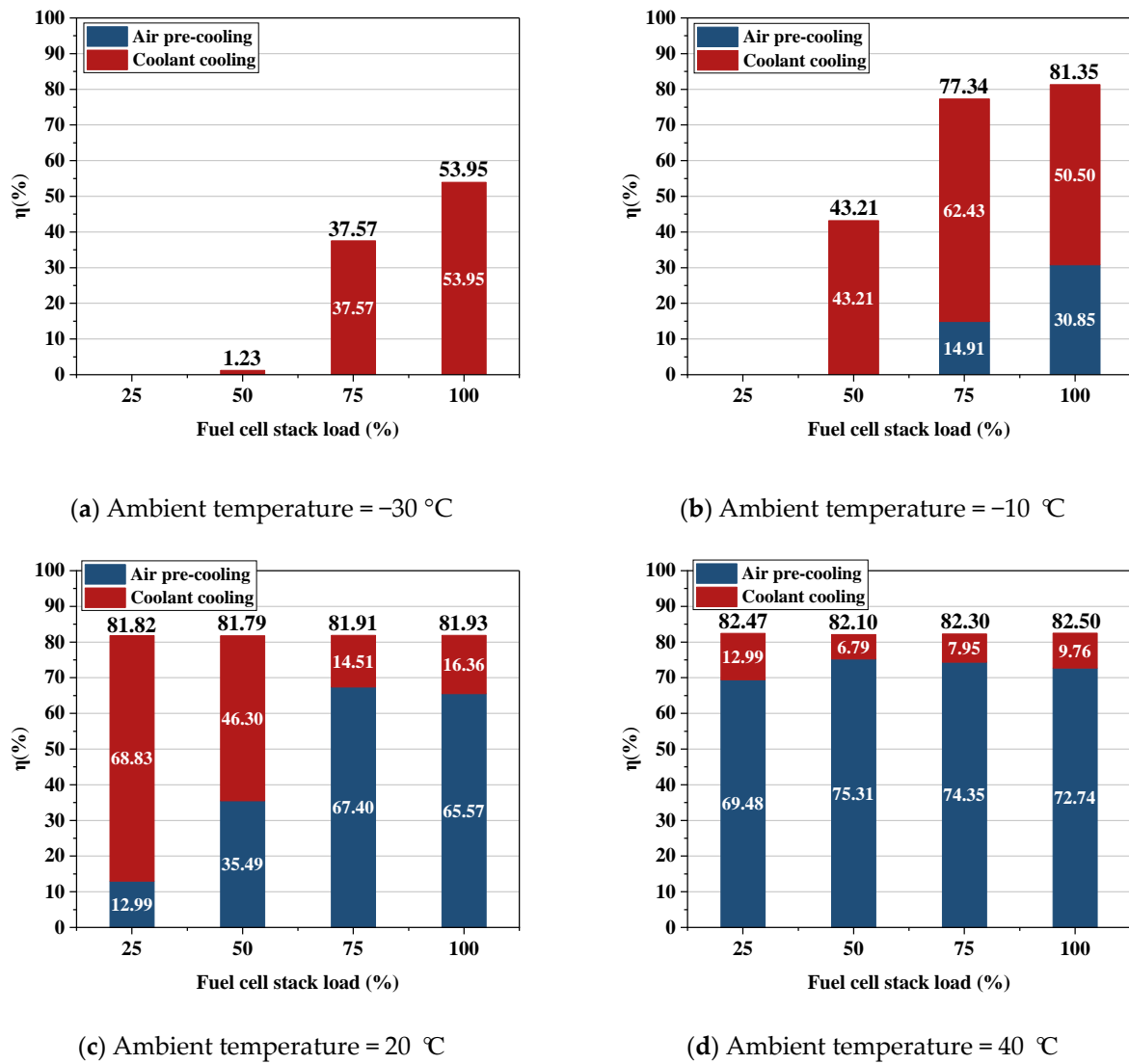


Figure 9. LH₂ cold energy utilization ratio. (a) Ambient temperature = -30 °C; (b) Ambient temperature = -10 °C; (c) Ambient temperature = 20 °C; (d) Ambient temperature = 40 °C.

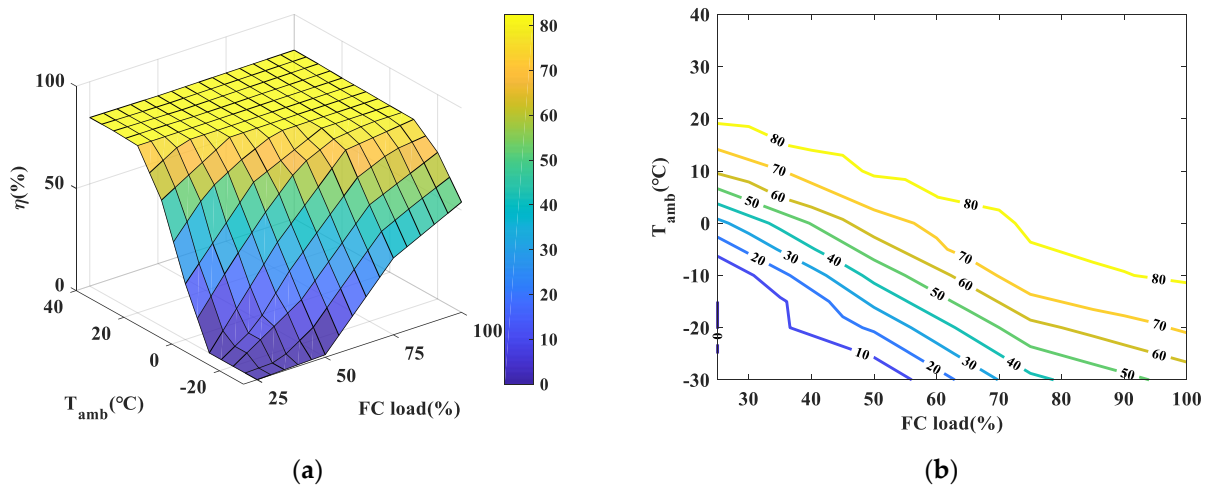


Figure 10. LH₂ cold energy utilization ratio results: (a) Cold energy utilization ratio as a function of ambient temperature and FC load; (b) Cold energy utilization system contour map.

4.2. Parasitic Power Saving Results

Compared to the original system without cold energy utilization, the parasitic power under different ambient temperatures (including $-30\text{ }^{\circ}\text{C}$, $-10\text{ }^{\circ}\text{C}$, $20\text{ }^{\circ}\text{C}$, and $40\text{ }^{\circ}\text{C}$) and fuel cell stack loads (25~100%) are shown in Figure 11.

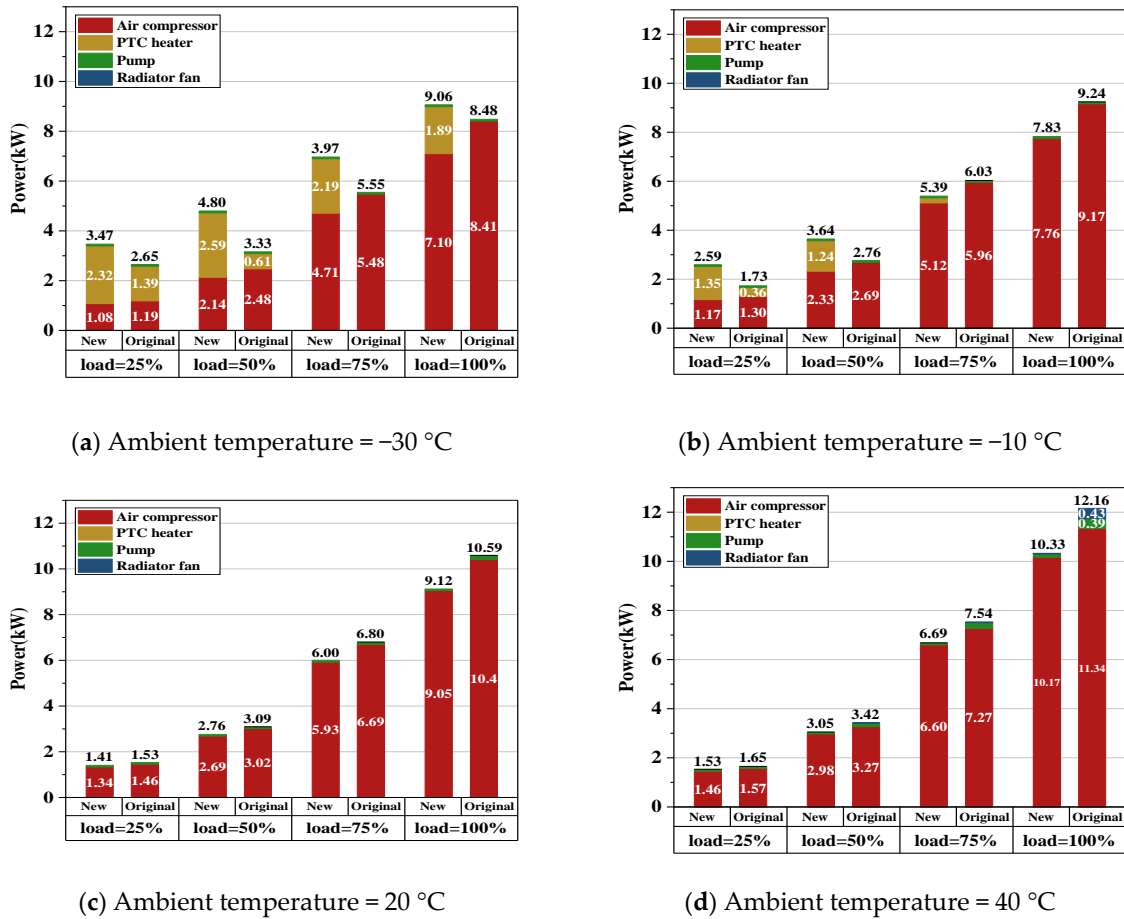


Figure 11. System parasitic power consumption. (a) Ambient temperature = $-30\text{ }^{\circ}\text{C}$; (b) Ambient temperature = $-10\text{ }^{\circ}\text{C}$; (c) Ambient temperature = $20\text{ }^{\circ}\text{C}$; (d) Ambient temperature = $40\text{ }^{\circ}\text{C}$.

At each stack load, the histogram on the left side (labeled as 'New') represents the parasitic power consumption of the LH_2 cold energy utilization system, and the histogram on the right side (labeled as 'Original') represents the parasitic power consumption of the original system. As shown in Figure 11a,b, it can be seen that, under low temperature ($< -10\text{ }^{\circ}\text{C}$) and light load ($< 50\%$), the power consumption of the heater (yellow column) of the original system accounts for a large proportion (up to 67% of P_{total}), indicating that the system does not have a suitable cooling demand and needs additional heat generation to meet thermal balance. Therefore, even though the cold energy utilization reduces air compressor power (red column), the reduction is limited compared to the increase in heater power, meaning that the total power consumption of the system may increase as a result. While at room temperature and higher (as shown in Figure 11c,d), the air compressor power increases and the heater stops working. Therefore, the use of cold energy can significantly reduce the air compressor power by decreasing the inlet temperature of compressor, which leads to obvious power saving (up to 1.4 kW), especially at a high load. As for the power of the water pump and radiator fan (green and blue columns), they account for a small part of the total power consumption. This is mainly because the maximum power consumption of the water pump and radiator fan is much smaller compared to the compressor power (about 5%). Thus, the power saving of the water pump and radiator fan is not significant, except under $40\text{ }^{\circ}\text{C}$ and a 100% load.

Figure 12a demonstrates the change of saving power with ambient temperature and a fuel cell stack load. The red plane is the 0-saving power base plane. The LH₂ cold energy utilization system can realize power saving except under low temperature and light load, and the saving power increases with temperature and load. The maximum saving power can achieve 1.8 kW (40 °C, 100% load), which is about 15% of the total parasitic power of the original system without cold energy utilization. Through a comparison of the saving power curve and 0-saving power base plane, the system can be divided into two states—a power saving state and a non-power saving state (as shown in Figure 12b). It can be seen that the load range corresponding to power saving increases with the temperature. The system is possible to realize power saving when the ambient temperature is above −25 °C and could save power in the whole load range when the temperature is above 16 °C. In addition, the heat load of the intercooler can also be reduced due to the temperature decrease of the compressed air. The maximum saving heat load is about 4.5 kW, which is about 50% of the intercooler heat load in the original system.

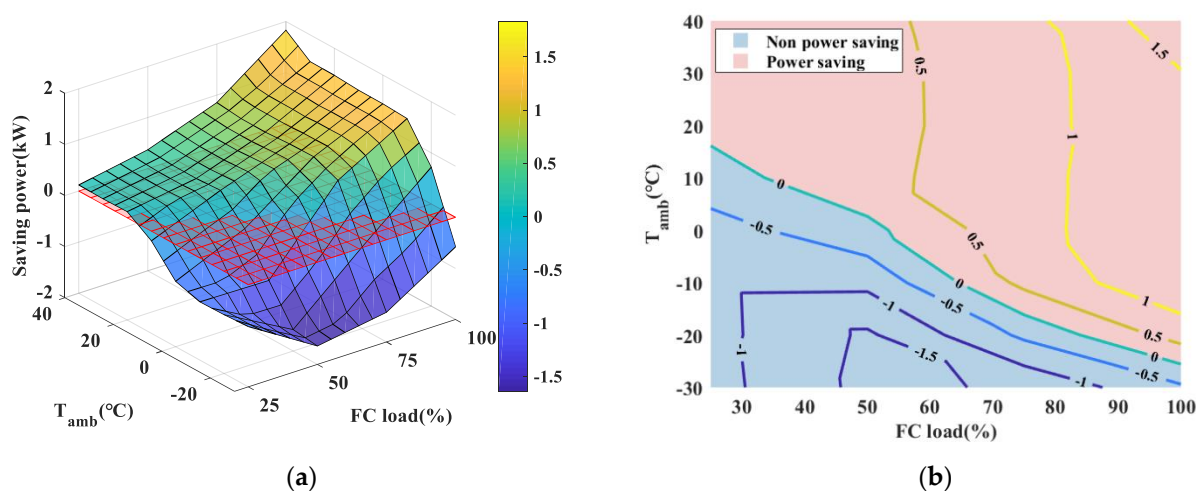


Figure 12. Total parasitic power saving results: (a) Saving power as a function of ambient temperature and FC load; (b) State division of the cold energy utilization system.

5. Conclusions

A kind of on-board liquid hydrogen cold energy utilization system is proposed and analyzed. By using two heat exchangers, the cold energy of LH₂ is utilized for cooling the inlet air of the compressor and the coolant of the accessories cooling system sequentially. A zero-dimensional model was established to analyze the performance of the system. The simulation results show that the cold energy utilization ratio can keep at a high level (above 80%), except under extremely low temperatures and light fuel cell stack load. Compared to the original LH₂ system without cold energy utilization, the new system could realize power saving when the ambient temperature was above −25 °C, and the maximum saving power achieved was 1.8 kW, which is about 15% of the total parasitic power. In addition, the intercooler heat load can also be reduced, which is beneficial as it reduces the size of the intercooler.

The on-board LH₂ cold energy utilization improves the overall efficiency of LH₂ and saves the system parasitic power consumption of heavy-duty fuel cell hybrid truck, which makes it more competitive as a fuel source. However, the analysis of the system is still preliminary, and the optimization of cold energy distribution between two heat exchangers needs to be simulated and verified. Other arrangements should be compared to explore the change of the inlet and outlet temperature of the heat exchanger and the impact on system's performance. Furthermore, the detailed control strategy of the system under different dynamic cycles is another important aspect in future research.

Author Contributions: Conceptualization, M.Y., S.H., F.Y. and L.X.; methodology, M.Y., S.H. and F.Y.; software, M.Y. and S.H.; validation, M.Y. and S.H.; formal analysis, M.Y. and S.H.; investigation, M.Y. and S.H.; resources, S.H., F.Y., L.X., Y.B. and D.Y.; data curation, M.Y., S.H., Y.B. and D.Y.; writing—original draft preparation, M.Y.; writing—review and editing, M.Y. and S.H.; visualization, M.Y.; supervision, F.Y. and L.X.; project administration, S.H., Y.B. and D.Y.; funding acquisition, S.H., Y.B. and D.Y. All authors have read and agreed to the published version of the manuscript.

Funding: This research was funded by the National Key Research and Development Program of China, grant number 2019YFB1504902.

Institutional Review Board Statement: Not applicable.

Informed Consent Statement: Not applicable.

Data Availability Statement: Not applicable.

Acknowledgments: This research was supported by Beijing Institute of Aerospace Testing Technology, Beijing SinoHytec Co., Ltd. and Beiqi Foton Motor Co., Ltd.

Conflicts of Interest: The authors declare no conflict of interest. The funders had no role in the design of the study; in the collection, analyses, or interpretation of data; in the writing of the manuscript, or in the decision to publish the results.

Nomenclature

Parameters and variables

E	Energy, J
F	Faraday constant, C/mol
h	Enthalpy, J/kg
I	Current, A
m	Mass, kg
\dot{m}	Mass flow rate, kg/s
M	relative molecular mass
N	Number
P	Power, W
S	Stoichiometric ratio
V	Electric potential, V
η	Efficiency
ω	Mass fraction of O ₂ in air

Subscripts

act	Activation
air	Air
$cell$	Fuel cell
$comp$	Compressor
$conc$	Convection
$coolant$	Coolant
$demand$	Cooling demand
$extra$	Excessive cold energy
fan	Radiator fan
$heater$	Heater
H_2	Hydrogen
LH_2	Liquid hydrogen
$nernst$	Nernst voltage
$ohmic$	Ohmic
O_2	Oxygen
$pump$	Water pump
$total$	Total parasitic power
$used$	Used cold energy
1	Heat exchanger 1
2	Heat exchanger 2

References

1. Li, M.; Bai, Y.; Zhang, C.; Song, Y.; Jiang, S.; Grouset, D.; Zhang, M. Review on the research of hydrogen storage system fast refueling in fuel cell vehicle. *Int. J. Hydrogen Energy* **2019**, *44*, 10677–10693. [[CrossRef](#)]
2. Abe, J.O.; Popoola, A.P.I.; Ajenifuja, E.; Popoola, O.M. Hydrogen energy, economy and storage: Review and recommendation. *Int. J. Hydrogen Energy* **2019**, *44*, 15072–15086. [[CrossRef](#)]
3. Helmolt, R.V.; Eberle, U. Compressed and Liquid Hydrogen for Fuel Cell Vehicles. In *Encyclopedia of Applied Electrochemistry*; Springer: Berlin/Heidelberg, Germany, 2014; pp. 245–253. [[CrossRef](#)]
4. Wang, Q.; Li, J.; Bu, Y.; Xu, L.; Qin, Z. Technical assessment and feasibility validation of liquid hydrogen storage and supply system for heavy-duty fuel cell truck. In Proceedings of the 2020 4th CAA International Conference on Vehicular Control and Intelligence (CVCI), Hangzhou, China, 18–20 December 2020.
5. Cardella, U.; Decker, L.; Klein, H. Roadmap to economically viable hydrogen liquefaction. *Int. J. Hydrogen Energy* **2017**, *42*, 13329–13338. [[CrossRef](#)]
6. Yilmaz, C. A case study: Exergoeconomic analysis and genetic algorithm optimization of performance of a hydrogen liquefaction cycle assisted by geothermal absorption precooling cycle. *Renew Energy* **2018**, *128*, 68–80. [[CrossRef](#)]
7. Cardella, U.; Decker, L.; Sundberg, J.; Klein, H. Process optimization for large-scale hydrogen liquefaction. *Int. J. Hydrogen Energy* **2017**, *42*, 12339–12354. [[CrossRef](#)]
8. Krasae-In, S.; Stang, J.H.; Neksa, P. Development of large-scale hydrogen liquefaction processes from 1898 to 2009. *Int. J. Hydrogen Energy* **2010**, *35*, 4524–4533. [[CrossRef](#)]
9. Kanbur, B.B.; Xiang, L.; Dubey, S.; Choo, F.H.; Duan, F. Cold utilization systems of LNG: A review. *Renew. Sustain. Energy Rev.* **2017**, *79*, 1171–1188. [[CrossRef](#)]
10. He, T.; Chong, Z.R.; Zheng, J.; Ju, Y.; Linga, P. LNG cold energy utilization: Prospects and challenges. *Energy* **2019**, *170*, 557–568. [[CrossRef](#)]
11. Liu, Y.; Han, J.; You, H. Performance analysis of a CCHP system based on SOFC/GT/CO₂ cycle and ORC with LNG cold energy utilization. *Int. J. Hydrogen Energy* **2019**, *44*, 29700–29710. [[CrossRef](#)]
12. Trevisani, L.; Fabbri, M.; Negrini, F.; Ribani, P.L. Advanced energy recovery systems from liquid hydrogen. *Energy Convers. Manag.* **2007**, *48*, 146–154. [[CrossRef](#)]
13. ZHANG, N.; LIOR, N. A novel Brayton cycle with the integration of liquid hydrogen cryogenic exergy utilization. *Int. J. Hydrogen Energy* **2008**, *33*, 214–224. [[CrossRef](#)]
14. Simcenter Amesim. Available online: <https://www.plm.automation.siemens.com/global/en/products/simcenter/simcenter-amesim.html> (accessed on 16 August 2021).